

# Application of PIV to AC Electrokinetic Flows

Dazhi Wang, Marin Sigurdson & Carl D. Meinhart

Department of Mechanical & Environmental Engineering  
University of California, Santa Barbara, CA 93106  
wangdz@engineering.ucsb.edu

## Abstract

An ac electric field is applied to induce particle and fluid motion in a wedge-shaped microchannel. Micron-Resolution Particle Image Velocimetry ( $\mu$ -PIV) is used to determine spatially resolved particle velocity and fluid velocity fields. Under steady state conditions, the particles experience a balance between dielectrophoretic forces induced by the non-uniform electric field and Stokes' drag forces due to viscous interactions with the fluid. The particle velocity is therefore different from the fluid velocity because of dielectrophoresis. A technique is developed, Two-Color  $\mu$ -PIV, to determine uniquely the *fluid* velocity from observation of particles without *a priori* knowledge of the electrical properties.

This technique is used to explore ac electrokinetically-generated fluid motion. A series of voltage levels at fixed frequency are applied to the wedge-shaped electrodes. The dependency of fluid velocity on applied voltage at different regions in the flow is obtained by fitting power-law curves. This is used to determine the underlying physical phenomena associated with ac electrokinetics. We found that both electrothermal effects and ac electroosmosis are important for the current experiment conditions. However, the electrothermal effect is dominant in the bulk fluid.

## 1. Introduction

In the presence of nonuniform electric fields, particles in a suspension experience dielectrophoretic (DEP) forces (Jones 1995). This force can move a particle towards areas of high-field or low-field strength, depending on difference of electrical properties between the particles and the suspending medium. These properties are a function of the frequency of the applied signal. Using microfabricated devices, manipulation of particles using DEP forces can be achieved in microscale channels on a chip with relatively small voltages. Dielectrophoresis has important applications in biological procedures, such as detecting, manipulating and separating bioparticles like cells, viruses, proteins and DNA (Bakewell et al. 1998; Morgan et al. 1999; Yang et al. 1999; Sigurdson et al. 2002).

While a nonuniform ac electric field can move suspended particles using dielectrophoretic forces, it can also move the fluid using the electrothermal effect or

ac electroosmosis (Ramos et al. 1998; Green et al. 2000; Ramos et al. 2000; Meinhart et al. 2002). Green et al. (2000) has conducted measurements of particle motion under the influence of non-uniform ac electric fields. Nonuniform electric fields produce spatially varying power densities in the fluid and therefore non-uniform temperature fields in the fluid, leading to local changes in conductivity and permittivity. The applied electric field interacts with gradients of conductivity and permittivity, giving rise to *electrothermal* forces in the liquid. In addition, ac electric fields produce double layers at the interface between the electrodes and the fluid. Ac electroosmosis occurs when the bulk fluid is put in motion by the action of the tangential component of the electric field on the induced double layers. Both the electrothermal effect and ac electroosmosis can be used to pump fluids or to turn on and off vortices in microfluidic devices without moving parts (Brown et al. 2001, Studeer et al., 2002). These can be used to actively separate, mix, or direct biological particles (Wong et al., 2003a, 2003b).

Micron-Resolution Particle Image Velocimetry ( $\mu$ -PIV) is a unique technique that allows detailed measurements of two-dimensional particle velocity and fluid velocity in microfluidic devices with spatial resolutions approaching one micron (Meinhart et al. 1999; Meinhart et al. 2000a; Meinhart et al. 2000b; Cummings 2000). Typically,  $\mu$ -PIV measures the fluid velocity by tracking the motion of fluorescent particles with an assumption that the small particles faithfully follow the fluid flow. In the current experiments, the particle velocity is different from the underlying fluid velocity, due to the DEP forces on the particles induced by the applied electric fields. The dielectrophoretic mobilities of particles and the fluid velocity can be measured using Two-Color  $\mu$ -PIV (Meinhart and Wang, 2001; Meinhart et al. 2002).

In this paper, we combine two-color fluorescent imaging with micron-resolution PIV to measure fluid velocity fields within a microfluidic device, subject to nonuniform ac electric fields. We compare the relative importance of the electrothermal effect to ac electroosmosis under certain experiment conditions.

## 2. AC Electrokinetics

Ac electrokinetics refers to the movement of particles and/or fluid induced by ac electric fields. The particles and the fluid may affect each other through viscous interaction. If the volume fraction of the particles is sufficiently low, the effect of the particles on the fluid is negligible.

### 2.1 Particle Motion

Under the influence of nonuniform electric fields, a particle in an aqueous medium experiences dielectrophoretic force and drag force. These forces are approximately balanced in steady state non-inertial flows, such that

$$\vec{F}_{DEP} + \vec{F}_D = 0, \quad (1)$$

where  $\vec{F}_{DEP}$  and  $\vec{F}_D$  are the forces due to DEP and Stokes' drag, respectively.

The time-averaged dielectrophoretic force on a homogeneous spherical particle is (Jones 1995)

$$\vec{F}_{DEP} = 2\pi\epsilon_m r^3 \text{Re}\{K\} \nabla |\vec{E}_{rms}|^2 \quad (2)$$

where  $\epsilon_m$  is the permittivity of the medium,  $r$  the particle radius,  $E_{rms}$  the root mean square of the ac electric field and  $K$  the Clausius-Mossotti factor given by

$$K = \frac{\epsilon_p^* - \epsilon_m^*}{\epsilon_p^* + 2\epsilon_m^*}, \quad (3)$$

where  $\epsilon^* = \epsilon - j\sigma/\omega$  is the complex permittivity,  $\sigma$  is the electrical conductivity, and subscripts  $p$  and  $m$  represent the particle and the suspending medium. The complex permittivity is a strong function of the frequency,  $\omega$ , of the applied signal.

The sign of the real part of the Clausius-Mossotti factor,  $\text{Re}\{K\}$ , defines positive ( $\text{Re}\{K\} > 0$ ) and negative ( $\text{Re}\{K\} < 0$ ) dielectrophoresis.  $\text{Re}\{K\}$  ranges from  $-0.5$  to  $1$ . The particles are moved toward the electric field intensity maxima by positive DEP forces and toward the minima by negative DEP forces.

The particles also experience drag forces due to viscous interactions with the fluid. In the current experiments, the Reynolds number is much less than  $1$ , with the characteristic fluid velocity scale of  $100\mu\text{m/s}$  and the characteristic length scale of  $50\mu\text{m}$ . The flow motion in the microchannel is not uniform, but we can assume the fluid velocity is uniform far from a particle, considering the diameter of the particle is only  $1\mu\text{m}$ . The drag force on a spherical particle follows Stokes' law

$$\vec{F}_D = 6\pi\mu r (\vec{u}_f - \vec{u}_p), \quad (4)$$

where  $\mu$  is the viscosity of the medium,  $\vec{u}_f$  is the fluid velocity and  $\vec{u}_p$  is the particle velocity.

## 2.2 Fluid Motion

The motion of incompressible fluid is governed by Stokes' equation, where the inertia terms are neglected, due to the near zero Reynolds number,

$$\mu \nabla^2 \vec{u}_f - \nabla p + \vec{f} = 0, \quad (5)$$

and the mass-conservation equation

$$\nabla \cdot \vec{u}_f = 0, \quad (6)$$

where  $p$  is the pressure and  $\vec{f}$  is a body force.

In our experiments the solid volume fraction of the working suspension is  $0.07\%$ . Therefore, the effect of the particles on the fluid is negligible. Subject to ac

electric fields, the fluid motion could be caused by the electrothermal effect, ac electroosmosis, or other unknown mechanisms.

### 2.2.1 Electrothermal Effect

Wedge-shaped electrodes produce non-uniform electric fields, resulting in non-uniform power density in the fluid and in turn, non-uniform temperature fields. Neglecting convective effects, which is reasonable at the microscale (Ramos et al. 1998), at steady state the temperature equation is obtained by balancing Joule heating with thermal diffusion

$$k\nabla^2 T + \sigma E^2 = 0, \quad (7)$$

where  $\sigma$  is the conductivity, and  $\sigma E^2$  represents the power density generated in the fluid by Joule heating from the applied electric fields. The electric field can be written in terms of the electric potential,  $E = -\nabla V$ , where the applied voltage field  $V$  in a charge neutral fluid obeys Laplace's equation,  $\nabla^2 V = 0$ .

The properties of the suspending medium are functions of temperature. The spatially varying temperature field leads to variation in properties such as charge density, electrical conductivity and permittivity. For the current experiment, natural convection arising from variation in fluid density is negligible. The electric fields interact with the gradients of permittivity and conductivity, giving rise to the electrothermal force that induces fluid motion. This phenomenon is termed the electrothermal effect. The time-averaged electrothermal force is expressed as (Ramos et al. 1998)

$$\bar{f}_E = -\frac{1}{2} \left[ \left( \frac{\nabla \sigma}{\sigma} - \frac{\nabla \varepsilon}{\varepsilon} \right) \cdot \bar{E}_0 \frac{\varepsilon \bar{E}_0}{1 + (\omega \tau)^2} + \frac{1}{2} |\bar{E}_0|^2 \nabla \varepsilon \right] \quad (8)$$

where  $E_0$  is the amplitude of the applied electric field,  $\omega$  is the applied frequency, and  $\tau = \varepsilon/\sigma$  is the charge relaxation time. The gradients of conductivity and permittivity are related to temperature by  $\nabla \varepsilon = (\partial \varepsilon / \partial T) \nabla T$  and  $\nabla \sigma = (\partial \sigma / \partial T) \nabla T$ .

Equations (5)-(8) describe the fluid motion caused by the electrothermal effect. The relation between the fluid velocity and the applied voltage can be estimated by order-of-magnitude analysis of these equations. It can be deduced that  $u_f \sim f_E$  from Eq. (5),  $\Delta T \sim V^2$  from Eq. (7) and  $f_E \sim (\Delta T)V^2$  from Eq. (8). Consequently, if the fluid motion is induced by electric fields due to the electrothermal effect, the magnitude of fluid velocity is proportional to the 4<sup>th</sup> power of the applied voltage, such that

$$u_f \sim V^4. \quad (9)$$

### 2.2.2 AC Electroosmosis

Similar to dc electroosmosis, fluid motion can also be induced by ac electric fields (Ramos et al. 1998; Green et al. 2000; Ramos et al. 2000). Double layers are formed at the interface between the electrodes and the fluid. The ions in the double layers are moved by electrical forces due to the non-zero tangential components of the electric fields at the edge of the double layer, which induce the bulk fluid motion. The sign of the ions in the double layers is always opposite to that of the charges on the corresponding electrode surfaces, which produces a cumulative effect under ac electric fields, and therefore results in steady-state fluid motion (Morgan & Green, 2003).

The scale of the double layer width is of order 1-10 nanometers, whereas the characteristic length of channels is of order micrometers, in the present investigation. Consequently, the bulk fluid motion due to ac electroosmosis can be described by Eqs. (5) and (6) with body force  $\bar{f} = \mathbf{0}$  and a finite velocity specified as the boundary condition at the electrode surface. The fluid velocity due to ac electroosmosis at the electrode surfaces is proportional to the square of the applied voltage (Green et al. 2000)

$$u_f \sim V^2. \quad (10)$$

## 3. Experiment Detail

### 3.1 $\mu$ -PIV Method

Micron-resolution Particle Image Velocimetry ( $\mu$ -PIV) has been developed to obtain quantitative measurements of spatially resolved fluid motion at microscale (Santiago et al. 1998; Meinhart et al. 1999; Meinhart et al. 2000a; Meinhart et al. 2000b; Cummings 2000; Meinhart & Wang 2001; Meinhart et al. 2002). This technique measures fluid motion by measuring the motion of fluorescent micron-sized tracing particles suspended in a transparent working fluid. Typically, it is assumed that the particles faithfully follow the fluid.

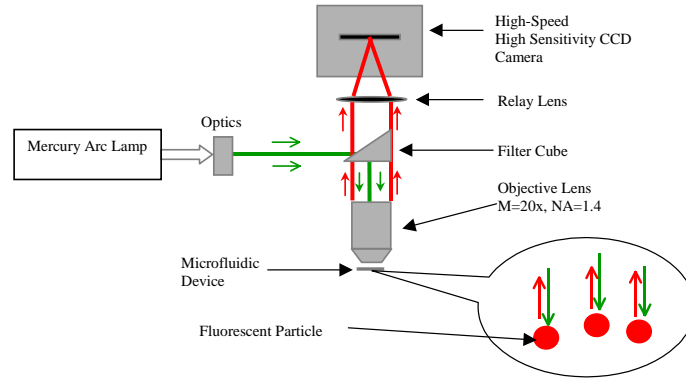


**Fig. 1.** view of the  $\mu$ -PIV system. The green lines represent the excitation light; the red lines represent the emitted fluorescent light.

In the current experiment, particle images are recorded using an epi-fluorescence microscope (*Model ECLIPSE E600FN, Nikon*) and a  $1280 \times 1024 \times 12$ -bit *Hamamatsu* CCD camera. Figure 1 shows a schematic of the  $\mu$ -PIV system. Continuous illumination light is provided by a mercury arc lamp, filtered by an excitation filter and transferred to the microfluidic device through the objective lens. The fluorescently-dyed particles in the fluid are excited and emit fluorescent light. The emitted light is passed through a barrier filter and delivered to a CCD camera. Time-sequences of images are correlated and then ensemble averaged to obtain 2-D velocity fields, following the technique developed by Meinhart et al. (2000b).

### 3.2 Two-Color $\mu$ -PIV

In the presence of nonuniform electric fields, dielectrophoretic forces cause the particle velocity to differ from the fluid velocity. However, if particle velocity fields are measured using two sets of electrically similar particles, but with two distinct sizes, under the same electric field and flow conditions, the fluid velocity can be determined uniquely. In order to distinguish between two different size sets of particles in PIV measurement, the different size particles are labeled with different color fluorescent dye.

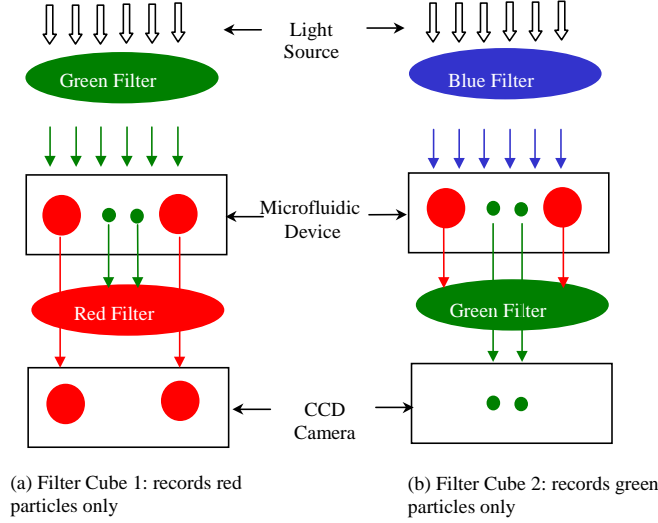


**Fig. 2.** Schematic of the process of the measurements using two-Color  $\mu$ -PIV. Two different size particles with different color can be recorded by adjusting the filter cube apparatus. This minimizes disturbances of the fluid experiment.

Figure 2 shows how choice of appropriate filters allows selective recording of either the large or the small particles by the CCD camera. When the filter cube assembly is positioned so that the green excitation and red barrier filters are activated, only the larger  $1\mu\text{m}$  particles are recorded. Positioning the filter cube assembly to activate the green excitation and blue barrier filters allows only the small  $0.7\mu\text{m}$  particles to be recorded by the CCD camera. Therefore, the flow experiment is not disturbed during the process of recording the images of different size particles.

For spherical particles, the magnitude of DEP force scales with radius cube (Eq. (2)), while the magnitude of the hydrodynamic drag force scales linearly with radius (Eq. (4)). Combining Eqs. (1), (2) and (4) gives the governing equations for two different size particles, but with similar electrical properties,

$$\varepsilon_m r_1^2 \text{Re}\{K\} \nabla \left| \vec{E}_{rms} \right|^2 + 3\mu(\vec{u}_f - \vec{u}_{p1}) = 0 \quad (11)$$

and

$$\varepsilon_m r_2^2 \text{Re}\{K\} \nabla \left| \vec{E}_{rms} \right|^2 + 3\mu(\vec{u}_f - \vec{u}_{p2}) = 0, \quad (12)$$

where  $u_{p1}$  and  $u_{p2}$  are the particle velocity fields, and  $r_1$  and  $r_2$  are the particle radii. The fluid velocity can be derived from the above two equations,

$$\vec{u}_f = \frac{\vec{u}_{p1} r_2^2 - \vec{u}_{p2} r_1^2}{r_2^2 - r_1^2}. \quad (13)$$

### 3.3 Microfluidic Device

A microfluidic device was designed and fabricated to produce electrokinetically-generated fluid motion in the observation plane. Figure 3 shows the test device. Two electrodes, separated by a  $50\mu\text{m}$  gap, are sandwiched between two glass wafers, forming a wedge-shaped  $550\mu\text{m}$  deep microchannel. The electrodes were fabricated on a  $550\mu\text{m}$  thick silicon wafer using PECVD, photolithography, deep RIE and e-beam evaporation. The microfluidic device was made at UCSB's *Nanofabrication Facility*. Figure 4 shows the fabrication process. By coating a silicon substructure with titanium and gold, we can produce electrodes that span the entire depth of the channel. Effective sidewall coverage was achieved with sample rotation through e-beam evaporation.

The ratio of the depth of the channel to the gap ( $550:50$ ) is sufficiently high so that we can assume the electric fields are two dimensional away from the top and bottom glass wafers. Two-dimensional particle and fluid motion is observed in the experiments. The measurement was focused on the region near the electrode apex, where the strong electric field can put the fluid into motion and produce detectable dielectrophoretic forces on particles.

A stabilized sweep generator (*model 22, Wavetek*) is used to provide ac signals, a stereo power amplifier (*model P500, David Hafler*) to amplify the voltage, and a digital phosphor oscilloscope (*model TDS3032, Tektronix*) to measure the frequency and voltage applied on the microelectrodes. The applied voltage ranged from  $11\text{-}14\text{V}_{\text{rms}}$ , with a frequency  $f = 200\text{kHz}$ . The test suspension is contained in a microfluidic device, and the fluid velocity fields are determined using Two-Color  $\mu\text{-PIV}$ .

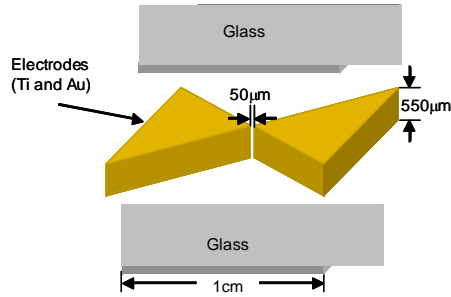


**Fig. 3.** Schematic diagram of the microfluidic device. An Si substrate is etched and Ti and Au is deposited on the Si substrate to form the electrode structure. The device is sandwiched by two glass wafers

Fluorescent polystyrene particles of two size sets were dispersed in a medium of 8.5% (w/v) sucrose and 0.3% (w/v) dextrose (to minimize electrolysis). The total volume fraction of the particles is 0.07%, with 0.02% for the  $1\mu\text{m}$  and 0.05% for the  $0.7\mu\text{m}$  particles. The Clausius-Mossotti factor  $\text{Re}\{K\}$  is  $-0.5$ . Therefore di-

electrophoresis is negative, which tends to push the particles away from intense electric fields, located at the electrode apex.

#### 4. Results and Analysis

Figures 5 and 6 show 2-D velocity fields of ac electrokinetic particle and fluid flows in the wedge-shaped micro-channel. The measurement domain is a  $415\mu\text{m} \times 415\mu\text{m}$  square, corresponding to  $1024 \times 1024$  pixels on the CCD camera. This measurement domain is  $150\mu\text{m}$  below the top glass wafer. The applied voltage is  $12\text{V}_{\text{rms}}$  with a frequency  $f = 200\text{kHz}$ , producing a non-uniform electric field across the wedge-shaped channel. Under the influence of this electric field, the particles were subjected to the mixed Stokes' drag and dielectrophoresis. Figure 5 shows the velocity fields of  $1\mu\text{m}$  and  $0.7\mu\text{m}$  fluorescent spherical particles, respectively. These two vector fields are raw PIV data resulting from averaging over 90 continuous images taken at a rate of 13 fps, without smoothing or removing erroneous velocity vectors. Figure 6 is the velocity field of electrokinetic fluid flow, determined uniquely from the two particle velocity fields using Eq. (13), without a priori knowledge of the 2-D electric field, the fluid properties, or the Clausius-Mossotti factor. Figs. 5A & 5b appear qualitatively similar to Fig. 6. However, the quantitative accuracy of the micro-PIV technique produces clear and measurable differences between these two velocity fields.

Figure 7 shows the direction and magnitude (within a constant) of the negative dielectrophoretic force on the particles, calculated according to Eq. 2. The similarity between the fluid and particle velocity fields (Figs. 5a, 5b & 6) indicates that

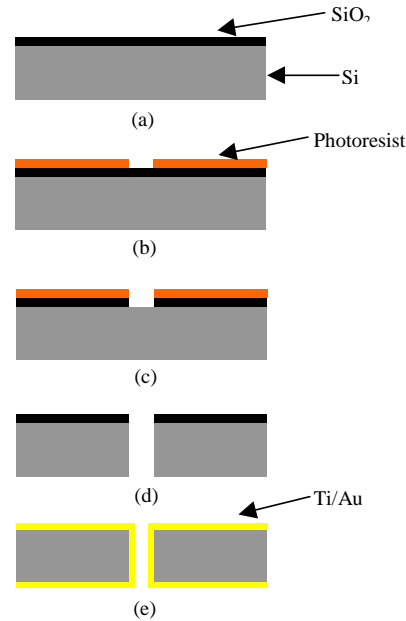


**Fig. 4.** Fabrication process for the electrode structure. (a) A  $3\mu\text{m}$  thick layer of  $\text{SiO}_2$  is deposited on a  $550\mu\text{m}$  thick silicon wafer by PECVD, (b) the pattern of the wedge-shaped channel is transferred to the photoresist through photolithography, (c) the sample is soaked in BHF for six minutes to remove the exposed  $\text{SiO}_2$ , (d) the wafer is etched through completely using Deep RIE, (e)  $500\text{\AA}$  Ti and  $4000\text{\AA}$  Au are deposited using e-beam evaporation.

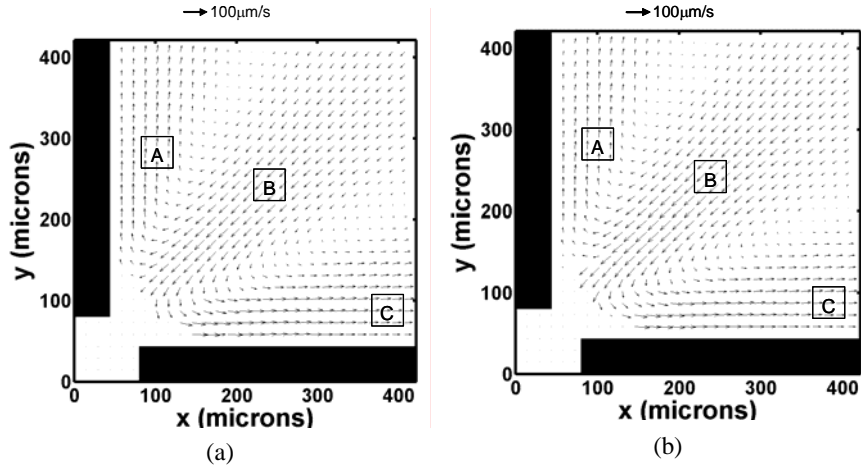


**Fig. 5.** Particle velocity fields obtained using two-color  $\mu$ -PIV. (a) The velocity field of the  $1\mu\text{m}$  diameter polystyrene particles; (b) the velocity of the  $0.7\mu\text{m}$  diameter polystyrene particles. The regions *A*, *B* and *C* are characteristic regions of the flow. The black rectangles represent the electrodes. The applied voltage is  $12V_{\text{rms}}$  at a frequency of  $200\text{ kHz}$ . These are raw data, i.e. no smoothing was applied.

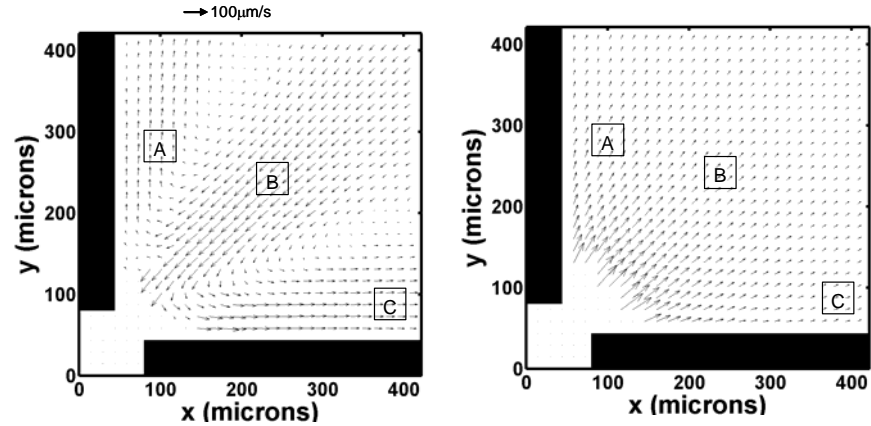


**Fig. 6.** The fluid velocity field, determined from the two particle velocity fields shown in Fig. 5 using Eq. (13). In the middle of the test device, fluid is drawn towards the electrode apex. Near the electrodes, the fluid moves away from the

**Fig. 7.** Numerical simulation of dielectrophoretic force field. Negative DEP will tend to move particles away from the electrode tips (i.e. away from high electric field intensity). The DEP forces near the electrode tips are not shown because their magnitudes are too large.

the influence of the fluid flow on the particles is dominant, compared to the influence of dielectrophoresis. If the DEP force were dominant, the particles would move away from the electrode tips in the directions shown in Fig. 7.

Although the particle and fluid flows are similar to one another, differences do exist. These differences are measured quantitatively using  $\mu$ -PIV's high spatial-resolution and accuracy. In Figs. 5, 6 & 7, the three regions *A*, *B* and *C* were selected as characteristic regions of the flow. Regions *A* and *C* are near the electrodes, and region *B* at the center of the flow. The magnitudes of the velocity vectors within each region are averaged and shown in Table 1, where  $u_{p1}$  is the velocity of  $1\mu\text{m}$  particles,  $u_{p2}$  the velocity of  $0.7\mu\text{m}$  particles and  $u_f$  the fluid velocity.

**Table 1.** Velocity in each region ( $\mu\text{m/s}$ ), for voltage  $12V_{\text{rms}}$ ,  $f = 200\text{kHz}$

	A	B	C
$u_{p1}$ ( $1\mu\text{m}$ )	65	107	88
$u_{p2}$ ( $0.7\mu\text{m}$ )	59	121	85
$u_f$	54	135	82

Table 1 shows that the particles are influenced by both fluid flow and dielectrophoresis. The particle velocity is similar to the corresponding fluid velocity in all the three regions, suggesting that the particle motion is strongly dominated by the fluid motion. However, there is a slight difference in velocity between the particles and the fluid, suggesting that dielectrophoresis has a small effect. According to Figs. 6 & 7, the fluid flow is in nearly the same direction as dielectrophoresis in regions *A* and *C*. Therefore all the particles are moving faster than the fluid. At region *B*, dielectrophoretic forces point opposite to the fluid flow, leading to the particles moving slower than the fluid. Table 1 also shows that the velocity of the larger particles is larger than that of the smaller particles at regions *A* and *C*, and the reverse is true at region *B*. This can be explained with Eq. (2), which indicates that the magnitude of the dielectrophoretic force scales with the cube of the particle radius. Accordingly, the  $1\mu\text{m}$  particles experience a three times larger dielectrophoretic force than the  $0.7\mu\text{m}$  particles, giving rise to the fact that the larger particles deviate from the fluid flow more than the smaller particles.

The flow pattern shown in Fig. 6 is similar to that caused by the electrothermal effect (Ramos et al. 1998; Meinhart and Wang 2001; Meinhart et al. 2002;), and by ac electroosmosis (Ramos et al. 1998; Green et al. 2000; Ramos et al. 2000). According to Eqs. (9) and (10), the fluid velocity scales with  $u_f \sim V^4$  if it is electrothermal effect, and with  $u_f \sim V^2$  if it is ac electroosmosis.

To determine which effect is dominant, we assume the fluid velocity obeys a power law, such that  $u_f \sim V^n$ . Fluid velocity in regions *A*, *B* and *C* were measured over a range of applied voltages,  $V = 2 - 14 V_{\text{rms}}$ , and  $n$  was found by fitting curves. Figure 8 shows the variation of the velocity with the applied voltage.

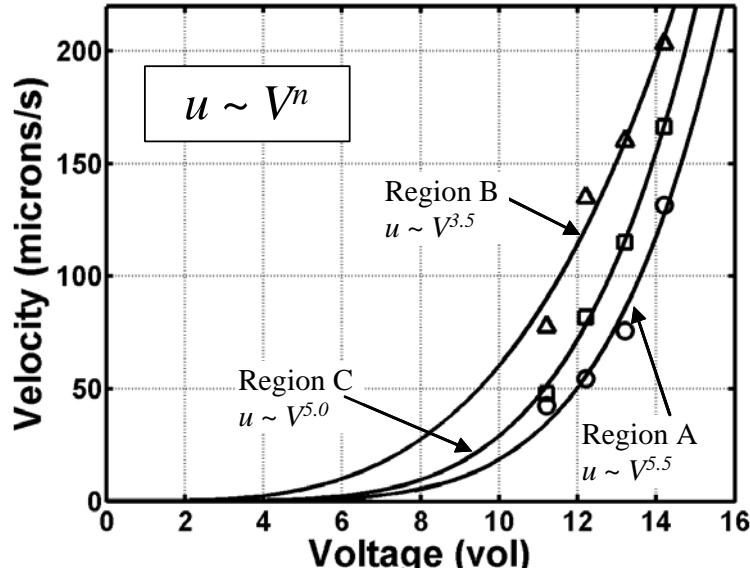


**Fig. 8.** Fluid velocity at different voltages. O represents averaged fluid velocity in region A,  $\Delta$  in region B and  $\square$  in region C. Fluid velocity  $u$  is assumed proportional to  $V^n$ , and  $n=3.5-5.5$ , and is found by the fitting curves.

The curve fitting reveals that at region B, around the center of the geometry,  $n \approx 3.5$ , which is close to 4, seeming to indicate dominance of electrothermally generated motion here. At regions A and C, near the electrodes,  $n \approx 5-5.5$ , which is a stronger dependence on voltage than either phenomena predicts. The fluid near the electrodes may be driven by a combination of the electrothermal effect and ac electroosmosis. In addition, there may be higher order effects occurring in the electric double layers, which are not accounted for in the simplified model developed by Ramos et al. (1998).

## 5. Conclusions

Decoupling of fluid velocity fields from observed particle velocity fields through Two-Color  $\mu$ -PIV in a 2-D wedge device allows the study of the various electrokinetic phenomena which affect particle and fluid motion: dielectrophoretic force on particles, ac electroosmotic force on the fluid surface, and electrothermal force on the fluid body.

The difference between particle and fluid velocity fields, as a result of DEP force on particles, was small, indicating a relative unimportance of DEP for this regime. The differences that did occur, however, agree qualitatively with the DEP force estimated based on fluid and particle properties.

The fluid velocity fields at different applied voltages were measured and compared in an effort to find the relation between the fluid velocity and the applied voltage. For current experimental conditions, the fluid velocity scales approximately with voltage to an exponential power of  $n \sim 3.5-5.5$ . This suggests that for the current experiments, electrokinetically-generated fluid motion may result from both the electrothermal effect and ac electroosmosis, and that the electrothermal effect is dominant in the bulk fluid.

## Acknowledgements

This work is supported by DARPA/ARMY DAAD 19-00-1-0400, DARPA/Air Force F30602-00-2-0609, NSF CTS-9874839 and NSF ACI-0086061.

## References

- Bakewell D, Hughes M, Milner J, Morgan H** (1998) Dielectrophoretic manipulation of avidin and DNA. Proceedings of the 20<sup>th</sup> Annual International Conference of the IEEE Engineering in Medicine and Biology Society, 20(2): 1079-1082.
- Brown, ABD, Smith CG, Rennie AR** (2001). Pumping of water with AC electric fields applied to asymmetric pairs of microelectrodes, *Phys. Rev. E*, 63, pp. 016305/1-8.
- Cummings E** (2000) An image processing and optimal nonlinear filtering technique for particle image velocimetry of microflows. Exp. in Fluids (Suppl.), 29(7): s42-s50
- Green N, Ramos A, Gonzalez A, Morgan H, Castellanos A** (2000) Fluid flow induced by nonuniform ac electric fields in electrolytes on microelectrodes-I. Experimental measurements. *Phys. Rev. E*, 61(4): 4011-4018.
- Jones T** (1995). Electromechanics of particles. New York: Cambridge University Press.
- Meinhart C, Wang D, Turner K** (2003) Measurement of AC Electrokinetic Flows. *Biomed. Microdevices*, 5(2): 139-145
- Meinhart C, Wang D** (2001) Accurate measurement of dielectrophoretic (DEP) mobility of particles and macromolecules. Proceedings of  $\mu$ -TAS 2001, Monterey, CA, October 21-25, 2001
- Meinhart C, Wereley S, Santiago J** (1999). PIV measurements of a microchannel flow. *Exp. in Fluids*, 27(5): 414-419.
- Meinhart C, Wereley S, Gray M** (2000a) Volume illumination for two-dimensional particle image velocimetry. *Meas. Sci. Technol.*, 11(6): 809 - 814.
- Meinhart C, Wereley S, Santiago J** (2000b) A PIV algorithm for estimating time-averaged velocity fields. *J. Fluids Eng.-T. ASME*, 122(2): 285-289
- Morgan H, Hughes M, Green N** (1999) Separation of submicron bioparticles by dielectrophoresis. *Biophys. J.*, 77: 516-525.

- Morgan H, Green N** (2003) AC Electrokinetics: colloids and nanoparticles, *Research Studies Press Ltd.*, Baldock, Hertfordshire, England.
- Ramos A, Gonzalez A, Green N, Castellanos A, Morgan H** (2000) Fluid flow induced by nonuniform ac electric fields in electrolytes on microelectrodes-II. A linear double-layer analysis. *Phys. Rev. E*, 61(4): 4019-4028.
- Ramos A, Morgan H, Green N, Castellanos A** (1998) Ac electrokinetics: a review of forces in microelectrode structures. *J. Phys. D: Appl. Phys.*, 31: 2338-2353.
- Santiago J, Wereley S, Meinhart C, Beebe D, Adrian R** (1998) A particle image velocimetry system for microfluidics. *Exp. in Fluids*, 25: 316-319
- Sigurdson M, Meinhart C, Wang D, Lui X, Feng J, Krishnamoorthy S, Makhijani V** (2002) Transport Enhancement in Tunable Laser Cavity Sensor. ASME – IMECE'02 MEMS Symposium, New Orleans, LA, Nov. 17–22, 2002
- Studeer V, Pepin A, Chen Y, Ajdari A** (2002). Fabrication of microfluidic devices for AC electrokinetic fluid pumping. *Microelectronic Engineering*, 61-62, pp. 915-920.
- Wong PK, Chen CY, Wang TH, Ho CM** (2003a) AC electroosmotic processor for biomolecules, In press *Transducers*.
- Wong PK, Wang TH, Deval JH, Ho CM** (2003b) Electrokinetics in micro devices for biotechnology applications, In Press *IEEE/ASME Transactions on Mechatronics*.
- Yang J, Huang Y, Wang X, Becker F, Gascoyne P** (1999) Cell separation on microfabricated electrodes using dielectrophoretic/gravitational field-flow- fractionation. *Anal. Chem.*, 71(5): 911-918.